JOURNAL OF GEOPHYSICAL RESEARCH, VOL. 87, NO. A1, PAGES 85-94, JANUARY 1, 1982

Energetic Electrons in the Magnetosheath and Upstream of the Bow Shock

J. W. BIEBER AND E. C. STONE

California Institute of Technology, Pasadena, California 91125

The characteristics and transport of >200 keV electrons upstream of Earth's bow shock and in the outer magnetosheath are studied using nearly 4 years of data from the California Institute of Technology Electron/Isotope Spectrometer aboard IMP 8. In the upstream region, elevated electron intensities ranging from near the background level ~0.1 $(cm^2\ s\ sr)^{-1}$ up to ~100 $(cm^2\ s\ sr)^{-1}$ are observed about 2% of the time and typically persist for less than 5 min. These burst electrons stream intensely ($\xi \sim 0.5$ to 1.5) sunward along the interplanetary magnetic field line. With the aid of a new coordinate system, it is demonstrated that the upstream bursts are most frequently seen on interplanetary field lines that trace to the inner magnetosheath, and that the total energy transported sunward by >200 keV upstream electrons averages $\sim 1.6 \times 10^{14}$ ergs/s, a figure comparable to the tailward energy flow observed in the permanent layer of energetic electrons adjacent to the magnetopause. Bursts of energetic electrons in the outer magnetosheath have time scales similar to those observed upstream, but they are typically ~10 times more intense and much less anisotropic ($\xi \lesssim 0.4$). The net flow of these electrons is toward the shock and very nearly equals the net flow away from the shock in the adjacent upstream region. The magnetosheath data suggest that energetic electron transport in this region may be described by a leaky box model with a scattering mean free path ~0.6 R_E. It is concluded that the energetic (>200 keV) component of upstream electrons originates downstream of the bow shock. Energetic electrons in the upstream region, in the outer magnetosheath, and in the magnetopause electron layer appear to be closely related and probably have a common origin in the inner magnetosheath or possibly the magnetosphere.

INTRODUCTION

Many of the energetic particles observed upstream of Earth's bow shock are believed to be accelerated locally, either by the shock itself or by wave-particle interactions. *Lin et al.* [1974] reported on 30–100 keV protons and suggested they were accelerated by waves on field lines connected to the shock. *Gosling et al.* [1978] noted two distinct populations of low energy ions: the diffuse population, which has a broad angular distribution and relatively flat energy spectrum, and the less common reflected population, which streams away from the shock and is restricted to energies ≲10 keV and which probably represents solar wind ions accelerated by interaction with the shock [*Sonnerup*, 1969; *Paschmann et al.*, 1980]. *Scholer et al.* [1979] studied upstream protons of energies 28–145 keV and concluded that they are the high-energy tail of the diffuse population.

Energetic (<30 keV) electrons in the upstream region were first noted by *Fan et al.* [1964] and were studied in more detail by *Anderson* [1968, 1969]. Recent results [*Anderson et al.*, 1979] suggest that these electrons are produced in a limited region near the point at which the interplanetary magnetic field is tangent to the shock surface.

Because energetic particles are produced in the magnetosheath and the magnetosphere as well as upstream of the bow shock, it is important to distinguish particles that originate in the magnetosheath or magnetosphere and subsequently propagate into the upstream region from particles that are accelerated by the shock or by upstream waves. *Sarris et al.* [1976] and *Krimigis et al.* [1978] reported observations of >290 keV protons and >220 keV electrons in the upstream region and suggested that their source lies within the magnetosphere. In a study of 40 keV to 2 MeV electrons in the magnetosheath and upstream, *Formisano* [1979*a*] concluded that these particles originate in the exterior cusp. Long-lived ion events (43 keV to 1.45 MeV) observed upstream of Jupiter's bow shock have characteristics similar to the terrestrial diffuse ions, but the Jovian ions appear to originate within Jupiter's magnetosphere, as evidenced by the presence of an enhanced component of heavy ions [*Zwickl et al.*, 1980].

One possible contributor to the upstream population of energetic electrons is the permanent layer of energetic electrons which lies adjacent to the magnetopause in the magnetosheath. This layer has been observed adjacent to the high latitude dayside magnetopause at energies >18 keV [*Meng and Anderson*, 1970, 1975], above the polar cap at energies >40 keV [*Domingo et al.*, 1977], and about the circumference of the distant magnetotail at energies >200 keV [*Baker and Stone*, 1977*a*, 1978]. Although the intensity of electron bursts within the layer varies greatly, elevated fluxes are almost continually observed on virtually every passage through the layer. In the distant magnetotail, the layer forms an annulus of thickness ~3 R_E about the magnetopause. In this region the electrons stream intensely tailward and may transport as much as 10^{18} ergs/s of energy [*Baker and Stone*, 1977*b*; *Stone et al.*, 1978]. Because the layer lies predominantly outside the magnetopause, where the field lines are open to the interplanetary medium, it is quite possible that some layer particles would propagate into interplanetary space.

The present report examines in detail the properties and the transport of energetic electrons in the outer magnetosheath as well as in the upstream region using >200 keV electron data collected by IMP 8 over a period of nearly 4 years. These data provide strong evidence that the high energy component of upstream electrons is closely related to the magnetopause electron layer.

DATA AND ANALYSIS

Data for this analysis were collected between 1973 day 303 and 1977 day 184 by the California Institute of Technology

Paper number 1A1070.
0148-0227/82/001A-1070$01.00

Electron/Isotope Spectrometer (EIS) aboard IMP 8 during 113 orbits at a distance ranging from 23 to 46 R_E from Earth. In the wide-geometry mode [see *Baker and Stone, 1977c*], the EIS separately accumulates counts of electrons >200 keV and >1 MeV for an 18-s period and reads out one measurement every 82 s. As the spacecraft spins with a period of about 2.6 s, the instrument scans the ecliptic plane and assigns each count to one of 8 angular sectors of 45° width.

In the wide-geometry mode, the EIS responds to >1 MeV protons as well as to >200 keV electrons. Consequently, periods during which an enhanced intensity level of energetic protons was present (as determined from EIS observations in the narrow-geometry mode) as well as periods during which the >200 keV electron background due to flare particles or Jovian electrons exceeded 0.1 $(\text{cm}^2\ \text{s}\ \text{sr})^{-1}$ were not included in the analysis. This resulted in the exclusion of approximately 50% of the available data.

For the purpose of this study, the streaming anisotropy was characterized by a vector which has GSE components

$$\xi_x = \frac{2}{N}\sum_i N_i \langle \cos \varphi \rangle_i \tag{1}$$

$$\xi_y = \frac{2}{N}\sum_i N_i \langle \sin \varphi \rangle_i \tag{2}$$

where N_i is the number of counts in the ith sector, N is the total number of counts summed over the 8 sectors, and φ is azimuth in the ecliptic plane. Angular brackets denote an average over the angular range of the ith sector. This definition was chosen because it provides a convenient method of characterizing the magnitude and direction of streaming without fitting the observed sectored rates to an assumed functional form. It can be shown that for an arbitrary pitch angle distribution, (1) and (2) give the correct streaming direction, provided that the field lies in the ecliptic plane. Moreover, the streaming anisotropy $\xi = (\xi_x^2 + \xi_y^2)^{1/2}$ calculated from (1) and (2) is, for most pitch angle distributions, a good approximation to the conventionally defined anisotropy

$$\xi' = \frac{3F}{UW} \tag{3}$$

where F is net streaming flux, U is density, and W is particle velocity. In fact, for first order anisotropies, for which the angular distribution $f(\theta)$ has the form

$$f(\theta) = f_0(1 + \xi' \cos \theta) \tag{4}$$

where f_0 is the omnidirectional intensity divided by 4π, the value of ξ calculated from (1) and (2) can be shown to equal exactly the value ξ' appearing in (4). However, for many of the electron bursts in the upstream region, the angular distribution is highly collimated ($\xi \gtrsim 1$) and cannot be expressed in first order form. In such cases, the value of anisotropy ξ given by (1) and (2) is slightly less than the conventional value ξ' given by (3). For the extreme case of a unidirectional beam of particles, (3) gives $\xi' = 3$, but (1) and (2) give $\xi \approx 2$. It should be noted that for these >200 keV electrons, which have velocities in excess of 200,000 km/s, the Compton-Getting anisotropy, caused by convection of the solar wind plasma, is only ~0.015.

Additional data available for this analysis are 15-s averages of magnetic field acquired by the IMP 8 magnetometer (R. P. Lepping and N. F. Ness, private communication, 1976). These data are used extensively to determine the relative configuration of Earth, the spacecraft, and the magnetic field and to identify bow shock crossings.

Data collected during the period mentioned above were used to assemble two large data sets upon which much of this report is based. The first data set, which will be referred to as the upstream data set, consists of 347,561 samples of energetic electron intensities and angular distributions (18-s averages centered 82 s apart) and magnetic field vectors (15-s average closest to the corresponding electron observation) observed in the upstream region over the entire range of the IMP 8 orbit from the dawn to the dusk bow shock. The second data set, which will be called the shock data set, partially overlaps the first and includes a total of 46,203 electron and field observations in the vicinity of the dawn bow shock from 12 hours before till 12 hours after the shock crossing. When multiple shock crossings occurred, data collected between the first and the last crossing were not considered. For both data sets, the times of shock crossings were determined separately on each orbit from an examination of the magnetic field data.

In this report, the term 'intensity,' denoted by j, refers (when not otherwise qualified) to the integral directional intensity of >200 keV electrons averaged over the spin plane. The units of intensity are $(\text{cm}^2\ \text{s}\ \text{sr})^{-1}$. The term 'flux,' denoted by F, is reserved for the net streaming flux in a given direction. Flux has units of $(\text{cm}^2\ \text{s})^{-1}$.

Energetic Electron Bursts Upstream of the Bow Shock

Figure 1 presents IMP 8 energetic electron data for an 8-hour period during which several unusually intense bursts were observed. At this time IMP 8 was more than 10 R_E upstream of the dawn shock, as illustrated at the lower left. The average magnetopause [*Formisano et al., 1979*] and bow shock [*Formisano, 1979b*] are also shown. The intensity of the energetic electron bursts, shown in the top panel of Figure 1, is extremely variable, often changing by more than a factor of 10 on a time scale of minutes. Below the intensity plot, the anisotropy vector is plotted for each observation above an intensity threshold of 0.5 $(\text{cm}^2\ \text{s}\ \text{sr})^{-1}$. Below this threshold, which corresponds to ~15 total counts, the calculated anisotropy becomes progressively less significant due to poor statistics. For the period shown, the anisotropy is typically ~1.0 to 1.6, and the direction of streaming is generally sunward along the Parker spiral field. At the lower right of Figure 1, the angular distribution observed during the particularly intense burst near 0710 is plotted (sunward down), along with the simultaneously observed magnetic field vector. The streaming is seen to be field aligned and highly anisotropic ($\xi \sim 1.6$), with almost no backscattered (earthward-moving) particles present.

The general characteristics of energetic electron bursts in the upstream region are summarized in Figure 2, which presents frequency of occurrence histograms of >200 keV electron intensity, anisotropy, and streaming direction for the upstream data set described in the previous section. The latter two histograms include only samples for which the intensity was ≥ 1 $(\text{cm}^2\ \text{s}\ \text{sr})^{-1}$, so that the background contribution could be neglected, and for which the field lay

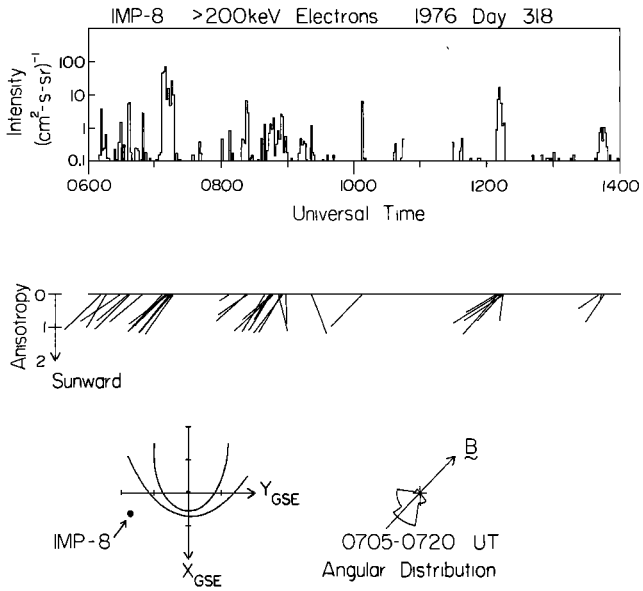

Fig. 1. Intensity and anisotropy of >200 keV upstream electrons during an 8-hour interval. Temporal resolution is 82 s. An intensity level of 1 $(cm^2\ s\ sr)^{-1}$ corresponds to about 29 total counts and has a relative error of ±19%. Spacecraft location is shown at bottom left, where tick marks on the axes indicate 20 R_E intervals. A sample angular distribution with magnetic field vector is shown at bottom right.

within 30° of the ecliptic plane, so that most pitch angles could be sampled. The intensity histogram in Figure 2 shows that bursts are a relatively rare occurrence, especially at the higher intensity levels. Intensities larger than 0.32 $(cm^2\ s\ sr)^{-1}$ are observed only 2.3% of the time. The anisotropy histogram exhibits a rather broad peak, extending from $\xi \sim 0.5$ to $\xi \sim 1.5$. The streaming direction histogram is rather sharply peaked at a GSE azimuth of −45°, corresponding to sunward flow along the Parker spiral field.

The location in the GSE coordinate system at which bursts were observed is shown in Figure 3. In the top graph a cross has been plotted in a plane representing the azimuth and Z coordinate of the spacecraft at 2-hour intervals for samples in the upstream data set. These points trace out the trajectory of IMP 8 during the nearly 4-year period of this study and show that the spacecraft has approximately uniform access to the upstream region within about 25 R_E of the ecliptic plane. Bursts of intensity ≥1 $(cm^2\ s\ sr)^{-1}$, by contrast, tend to occur dawnward of the Earth-sun line, as the lower plot in Figure 3 shows. This feature, which is common to many upstream particle species, appears because, for a nominal Parker spiral field, points duskward of the Earth-sun line often are not connected to the bow shock along the magnetic field line. Aside from the dawn-dusk asymmetry, no dependence of bursts upon location is evident in Figure 3. In fact, bursts do exhibit an additional dependence upon geometry, more restrictive than simple connection to the shock. To demonstrate this dependence it is necessary to introduce a new coordinate system.

GIPM Coordinates

The greatest likelihood of observing a >200 keV electron burst occurs on those interplanetary field lines that penetrate most deeply into the magnetosheath. To demonstrate this geometric effect, a new coordinate system, called geocentric interplanetary medium (GIPM) coordinates, was developed which is more convenient for mapping interplanetary field lines into the magnetosheath than more commonly used coordinate systems. The GIPM system is obtained by rotating the GSE system about the X axis in such a way that two conditions are satisfied: (1) the Z component of the interplanetary magnetic field vanishes in the new coordinate system, and (2) the azimuth of the interplanetary field in the new system lies in the second (90° to 180°) or the fourth (270° to 360°) quadrant of the X_{GIPM}-Y_{GIPM} plane. In general, there are two rotation angles separated by 180° that satisfy the first condition, but only one of these also satisfies the second condition. If (B_X, B_Y, B_Z) are the components of the interplanetary magnetic field in the GSE system, then the coordinate transformation that satisfies the above conditions is

$$X_{GIPM} = X_{GSE} \tag{5}$$

$$Y_{GIPM} = Y_{GSE} \cos\alpha + Z_{GSE} \sin\alpha \tag{6}$$

$$Z_{GIPM} = -Y_{GSE} \sin\alpha + Z_{GSE} \cos\alpha \tag{7}$$

where

$$\alpha = \tan^{-1}(B_Z/B_Y) + 180° \qquad B_X B_Y \geq 0$$
$$\alpha = \tan^{-1}(B_Z/B_Y) \qquad B_X B_Y < 0 \tag{8}$$

Equation (8) is valid when B_Y is nonzero. If $B_Y = 0$, then $\alpha = 270°$ if $B_X B_Z \geq 0$ and $\alpha = 90°$ if $B_X B_Z < 0$.

The advantages of the GIPM coordinate system are illustrated in Figure 4. Figures 4*a* through 4*c* show a spacecraft located at a fixed point in the GSE system for 3 orientations of the interplanetary magnetic field, and Figure 4*d* shows the

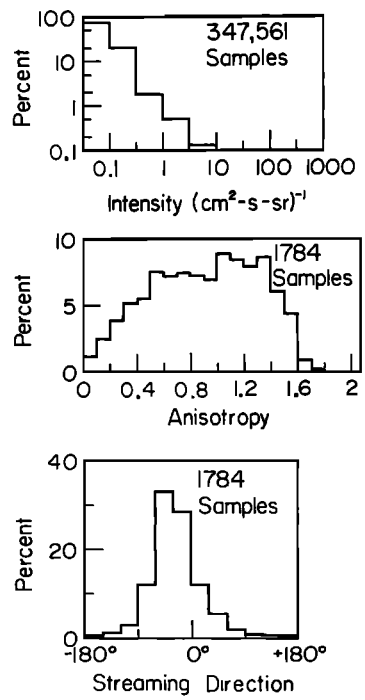

Fig. 2. Frequency of occurrence histograms of >200 keV electron intensity, anisotropy, and streaming direction in the upstream region. For the intensity histogram, axes are logarithmic. The leftmost bin includes all samples of intensity <0.1. Error bar (absolute) on the anisotropy of an individual sample is typically ±0.2 units. Streaming direction is the GSE azimuth of the anisotropy vector. Hence 0° corresponds to sunward flow.

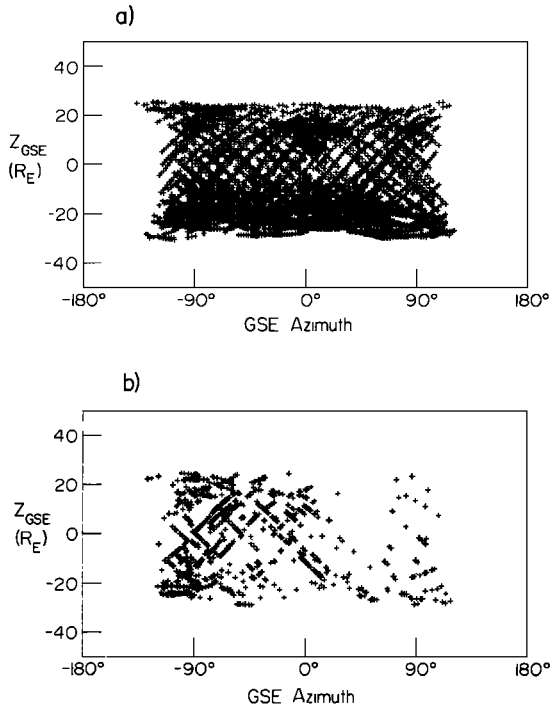

Fig. 3. GSE plots of (*a*) spacecraft trajectory and (*b*) positions at which burst intensities ≥ 1 (cm^2 s sr)$^{-1}$ were observed in the upstream region between 1973 day 303 and 1977 day 184.

same 3 configurations plotted in the GIPM system. In all cases the X component of the field is assumed to be negative (inward in the figure). Several features of the GIPM system should be noted:

1. The projections of the interplanetary field lines into the Y_{GIPM}-Z_{GIPM} plane are always horizontal lines. While in the GSE system the spacecraft remains fixed as the field changes orientation, in the GIPM system it is the field that remains fixed as the spacecraft rotates about the X axis.

2. For comparable values of Y_{GIPM}, it is the Z_{GIPM} coordinate of the spacecraft that determines how well the spacecraft is connected to Earth along the field line. Essentially, Z_{GIPM} is the impact parameter with Earth of the field line on which the spacecraft is located. Thus Figure 4*a*, for which $Z_{GIPM} = 0$, illustrates the most favorable connection, and Figure 4*b* illustrates a less favorable one. This feature of the GIPM system is preserved in models that take into account the distortion of field lines in the magnetosheath. According to gasdynamic theory [*Alksne*, 1967], the field lines that probe most deeply into the magnetosheath are those with the smallest values of $|Z_{GIPM}|$. Interplanetary field lines with $Z_{GIPM} = 0$ are convected directly toward Earth and experience the greatest amount of distortion in the magnetosheath. The gasdynamic models predict that these field lines trace to points directly adjacent to the magnetopause. Field lines with larger values of $|Z_{GIPM}|$ experience less distortion, do not penetrate as deeply, and ultimately slip up over the top of the magnetopause or below it.

3. Points in the $Y_{GIPM} < 0$ hemisphere are more favorably connected to the inner magnetosheath than points in the opposite hemisphere. In the GSE system, the dawn hemisphere ($Y_{GSE} < 0$) is normally better connected than the dusk hemisphere, where many field lines may not even intersect the shock. However, when the field departs substantially from the Parker spiral direction, this asymmetry may reverse, and the dusk hemisphere may be better connected. As a result of the requirement that the azimuth of the interplanetary field lie in the second or fourth quadrant of the X_{GIPM}-Y_{GIPM} plane, the ambiguity as to which hemisphere is better connected does not exist in the GIPM system. Thus, under certain conditions, a spacecraft located in the dusk hemisphere may transform to the $Y_{GIPM} < 0$ (more favorably connected) hemisphere. Conversely, a spacecraft located in the dawn hemisphere may transform to the $Y_{GIPM} > 0$ (less favorably connected) hemisphere, as illustrated by Figure 4*c*.

Dependence of Bursts Upon GIPM Coordinates

In Figure 5 the tendency of bursts to occur at small values of $|Z_{GIPM}|$, corresponding to field lines that probe deeply into the magnetosheath, is demonstrated. Figure 5*a* shows the Z_{GIPM} coordinate and azimuth (measured from the $+X_{GIPM}$ axis in the X_{GIPM}-Y_{GIPM} plane) of the spacecraft at 2-hour intervals for samples in the upstream data set. The trajectory trace is not smooth because the interplanetary field, and hence the GIPM coordinate, can vary significantly in the course of 2 hours. Figure 5*b* shows the locations at which bursts of intensity ≥ 1 (cm^2 s sr)$^{-1}$ were observed. The circular structure near the center represents a series of bursts which occurred over a period of several hours. Variations in the orientation of the interplanetary magnetic field during this period caused the bursts to be distributed in a circular pattern centered on the X axis (see Figure 4*d*).

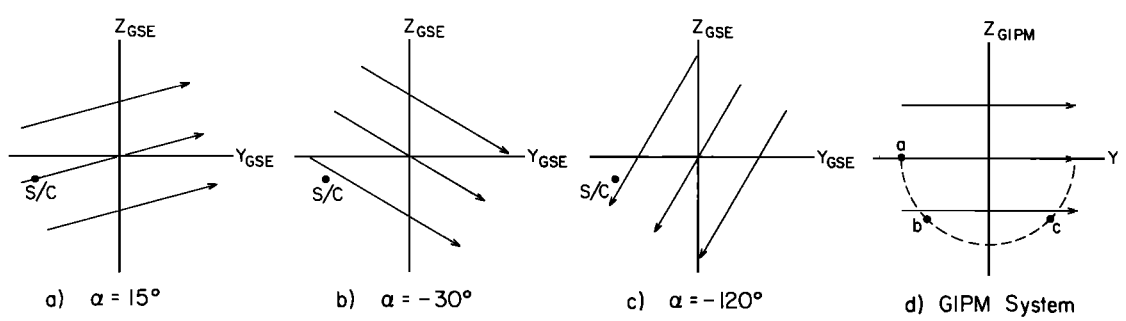

Fig. 4. The first 3 panels show a spacecraft (S/C) at a fixed position in the Y_{GSE}-Z_{GSE} plane for various orientations of the interplanetary field. The X component of the field is taken to be negative. The angle α is the rotation angle from GSE to GIPM coordinates. Figure 4*d* shows the same 3 field/spacecraft configurations (Figures 4*a*, 4*b*, 4*c*) as they appear in the GIPM system.

Although points within ~30 R_E of $Z_{GIPM} = 0$ are approximately uniformly represented in the upstream data set, as Figure 5*a* demonstrates, the bursts are mostly confined to a smaller region, as Figure 5*b* shows. Because points with $Y_{GIPM} > 0$ often do not connect with the shock, few bursts are observed in the $Y_{GIPM} > 0$ hemisphere, a dependence that is also evident in GSE coordinates (Figure 3). An additional dependence upon field geometry, which is not revealed in GSE coordinates, is the tendency for bursts to occur at $|Z_{GIPM}| \lesssim 15\ R_E$. This dependence, which is more restrictive than simple connection of the field line to the shock, suggests that the source of >200 keV upstream electrons lies in the inner magnetosheath or possibly the magnetosphere.

The dependence of bursts upon field geometry is exhibited more quantitatively in Figure 5*c*, which shows via a gray scale the probability, as a function of position, of observing a burst of intensity ≥ 0.32 (cm^2 s sr)$^{-1}$. To obtain this plot, the GIPM coordinate system was divided into bins of size 6° × 4 R_E, and the number of bursts in each bin was divided by the total number of observations in the bin, yielding the probability of observing a burst. For improved statistics, a lower burst threshold was used than in Figure 5*b*, and only the absolute value of Z_{GIPM} was considered. The probability attains a maximum value of 17% in the bin extending from −96° to −90° azimuth and from $|Z_{GIPM}| = 0$ to 4 R_E and decreases fairly smoothly away from this peak. The peak probability of 17%, though well above the overall upstream value of 2%, is somewhat smaller than might be expected if the field lines in this region trace directly to the magnetopause electron layer, where intensity levels >0.32 (cm^2 s sr)$^{-1}$ are almost continuously observed. Two reasons may be cited for this. First, use of the GIPM coordinate system to trace field lines is valid only insofar as the local field measured at IMP 8 is representative of the global field between the spacecraft and Earth. Fluctuations of the interplanetary field on a scale of $\lesssim 30\ R_E$ will disperse the bursts over a wider area and decrease the peak probability of observing a burst. Second, electrons that propagate from the magnetosheath into the upstream region experience a reduction of spin-averaged intensity by a factor of ~10 at the shock, as will be shown in the next section. Thus, most bursts with intensities $\lesssim 3$ (cm^2 s sr)$^{-1}$ in the magnetosheath will fall below the burst threshold of 0.32 (cm^2 s sr)$^{-1}$ after propagating across the shock.

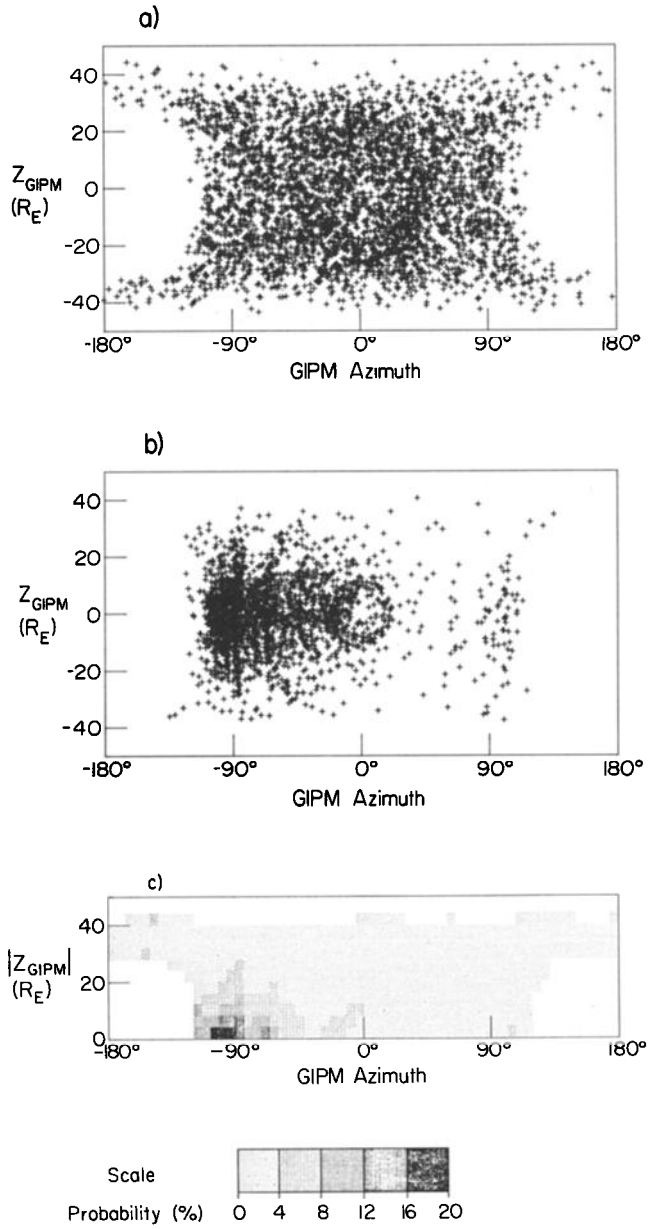

Fig. 5. GIPM plots of (*a*) spacecraft position at 2-hour intervals for the upstream data set, (*b*) positions at which burst intensities ≥ 1 (cm^2 s sr)$^{-1}$ were observed, and (*c*) probability of observing a burst of intensity ≥ 0.32 (cm^2 s sr)$^{-1}$.

Assuming a Parker spiral geometry (field azimuth of −45° or +135°), and noting that the observations were made at a radial distance ~35 R_E, the point of maximum probability in Figure 5*c* connects to the shock at about $X_{GIPM} = -8.1\ R_E$, $Y_{GIPM} = -28.6\ R_E$. Thus the greatest flow of particles across the shock apparently occurs somewhat tailward of Earth.

The intensity of >200 keV upstream electrons does not depend strongly upon distance from the shock. This can be seen to some extent in Figure 5*c*. For the average shock position and the average spacecraft radial distance, the peak probability near −90° corresponds to a distance about 8 R_E from the shock. Points at more negative values of azimuth are closer to the shock on average, yet the probability of observing a burst is less. Evidently the dependence of bursts upon distance from the shock is minor compared to the azimuthal dependence over this radial and azimuthal range. The possibility of a distance dependence was investigated in more detail by examining data acquired near the X_{GIPM}-Y_{GIPM} plane separately for different radial and azimuthal ranges. The data show the region of highest burst occurrence to be a band, approximately aligned with the Parker spiral direction, which intersects the shock around the point of maximum flow mentioned above. No evidence of a strong dependence of bursts upon distance is evident over the radial range 23 to 46 R_E. This result is not unexpected, since the highly anisotropic angular distributions exhibited by upstream electrons suggest that they propagate almost scatter-free, and intensity does not depend upon distance in scatter-free transport.

Evidence that upstream bursts are related to the magnetopause electron layer is provided by a comparison of the total net flux of particles away from Earth in the upstream region with the total net tailward flux observed in the layer. Figure

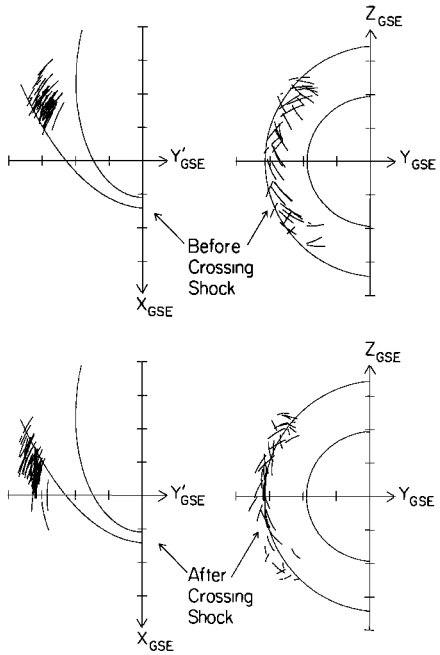

Fig. 6. Spacecraft trajectory for the 12-hour period before (top) and after (bottom) the dawn shock crossing. Tick marks show 10 R_E intervals. For the ecliptic plane projection, the nominal shock and magnetopause are shown, and spacecraft positions have been rotated into the ecliptic plane—i.e., $Y_{GSE}' \equiv -(Y_{GSE}^2 + Z_{GSE}^2)^{1/2}$. In the Y_{GSE}-Z_{GSE} plane, representative cross sections (corresponding to $X_{GSE} = -13\ R_E$) of the nominal bow shock and magnetopause are shown. However, actual shock crossings occurred over a range of X_{GSE}.

5c shows that the orbit of IMP 8 intercepts most of the upstream flow, since the peak probability lies well within the upstream region accessible to IMP 8. Figure 5c also suggests that the upstream data set is large enough to yield a representative average of this temporally variable flow, because, if temporal variations were the dominating factor, a well-defined spatial region in which bursts preferentially occur would not have appeared. To perform the calculation of average total net flux, the coordinate grid in Figure 5c was assumed to represent the surface of a cylinder of radius 35 R_E centered on Earth and perpendicular to the X_{GIPM}-Y_{GIPM} plane. For a given burst, the component of net flux normal to the surface of the cylinder is $4\pi j(\xi/3)\cos\eta$, where j is the spin-averaged directional intensity, ξ is the anisotropy, and η is the angle between the streaming direction and the outward normal of the cylinder. If angular brackets denote averaging over all bursts of intensity ≥ 0.32 (cm^2 s sr)$^{-1}$ within the ith bin, then the total net flow Q of electrons away from Earth is

$$Q = \sum \langle 4\pi j(\xi/3)\cos\eta\rangle_i P_i A_i \qquad (9)$$

where P_i is the probability of observing a burst of intensity ≥ 0.32 (cm^2 s sr)$^{-1}$ in the ith bin, and A_i is the area encompassed by the bin ($\sim 30\ R_E^2$, taking into account that negative as well as positive Z_{GIPM} values are included within each bin). The summation is over all bins in the upstream region. The result of this calculation is that on average $\sim 2.7 \times 10^{20}$ electrons per second stream away from Earth in the upstream region. For a spectral index of 3.2 (see below), the average energy of these >200 keV electrons is $\langle E\rangle = 370$ keV. Hence, the total energy transported sunward by these particles is $\sim 1.6 \times 10^{14}$ ergs/s on average. Based on a study of 101 crossings of the magnetopause electron layer adjacent to the distant magnetopause, *Baker and Stone* [1977*b*] concluded that the total energy transported tailward by >200 keV electrons in the layer ranges from $\sim 10^{14}$ to $\sim 10^{15}$ ergs/s. Although *Baker and Stone* [1977*b*; see also *Stone et al.*, 1978] also suggested that this flow could be extrapolated downward in energy to ~1 keV, yielding a total flow $\sim 10^{18}$ ergs/s, the comparison of energy flows made here is based only upon the flow of >200 keV electrons in the layer, which Baker and Stone observed directly.

Additional evidence for a relationship between upstream electrons and layer electrons is provided by a comparison of energy spectral indices in the two regions. Under the assumption that the differential intensity J obeys a power law ($J \propto E^{-\gamma}$, where E is energy), the spectral index γ can be determined from a comparison of average count rates in the >200 keV and the >1 MeV energy channels. For upstream bursts, the average value of γ was found to be 3.2, identical to the average value of γ obtained for bursts in the magnetopause electron layer [*Baker and Stone*, 1978].

Based upon the equality of spectral indices for layer and upstream electrons, upon the similarity of the total layer and the total upstream flow of >200 keV electrons, and upon the dependence of upstream bursts on field geometry, it is concluded that energetic electron bursts in the upstream region occur on the sunward extension of the field lines adjacent to the magnetopause which thread the magnetopause electron layer and that the upstream bursts are supplied by the same source that supplies the layer.

Transport of Electrons Through the Magnetosheath and Across the Bow Shock

As a consequence of the interpretation that energetic upstream electrons originate in the inner magnetosheath, it

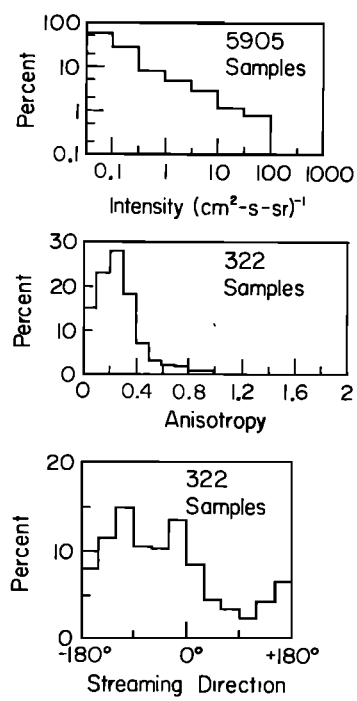

Fig. 7. Frequency of occurrence histograms of >200 keV electron intensity, anisotropy, and streaming direction in the outer magnetosheath (3-hour interval before shock crossing). Format is the same as in Figure 2.

should be possible to observe these electrons streaming toward the shock in the outer magnetosheath. In a previous report [*Bieber and Stone,* 1979] electron data for a single traversal of the magnetosheath were presented which showed that the streaming direction shifts from tailward in the magnetopause electron layer to dawnward in the outer magnetosheath and finally to sunward in the upstream region. With the aid of the shock data set described above, this result will now be shown to be characteristic of the nearly 4 years of IMP 8 data used in this study. It will be demonstrated that >200 keV electrons in the outer magnetosheath generally stream toward the shock and, furthermore, that the average net flow toward the shock equals almost exactly the net flow away from the shock observed in the upstream region.

Figure 6 shows segments of the IMP 8 trajectory on 44 orbits for the 12-hour interval before crossing the dawn shock (upper graphs) and the 12-hour interval after crossing the dawn shock (lower graphs). For the plots on the left, the spacecraft position has been rotated into the ecliptic plane. The average shock and magnetopause are also shown, though the actual shock crossing was determined separately on each orbit from the magnetic field data. These plots show that the shock data set consists predominantly of data collected tailward of Earth ($X_{GSE} \sim -5$ to $-20\ R_E$) over a wide range of displacements from the ecliptic plane ($Z_{GSE} \sim -25$ to $+25\ R_E$). Typically, the shock is crossed at about $X_{GSE} \sim -13\ R_E$, somewhat tailward of the point of maximum electron flow ($\sim -8\ R_E$) noted in connection with Figure 5. Bursts in the outer dusk magnetosheath will not be considered here, because they are observed far less frequently than bursts on the dawn side.

The properties of >200 keV electron bursts in the outer magnetosheath are summarized in Figure 7, which presents frequency of occurrence histograms of intensity, anisotropy, and streaming direction for only the 3-hour interval before the shock crossing. As in Figure 2, the anisotropy and direction histograms include only samples of intensity ≥ 1 $(\text{cm}^2\ \text{s}\ \text{sr})^{-1}$ for which the field lay within 30° of the ecliptic plane. Comparison of Figure 7 and Figure 2 shows that bursts of a given intensity are seen ~10 times more frequently in the outer magnetosheath than upstream. Intensity levels ≥ 0.32 $(\text{cm}^2\ \text{s}\ \text{sr})^{-1}$ are seen 17% of the time in the outer magnetosheath, as compared with 2.3% of the time upstream. The anisotropy in the outer magnetosheath tends to be much less than upstream, the majority of samples having $0.1 < \xi < 0.4$. Most samples have a streaming direction between −180° and 0°. This broad distribution centered on −90° (dawnward) is consistent with a source in the inner magnetosheath. Caution should be used in interpreting these anisotropy data, because small values of anisotropy can be generated by statistical fluctuations in the sectored count rates. For example, at an intensity level of 3 $(\text{cm}^2\ \text{s}\ \text{sr})^{-1}$, corresponding to ~88 total counts, there is a 47% probability that an isotropic distribution will yield an anisotropy $\xi > 0.2$ due to statistics [*Marshall,* 1977]. However, even though the streaming direction derived for an individual sample is rather uncertain, the distribution of streaming directions exhibited in Figure 7 indicates that there is a statistically significant average flow direction.

To characterize the average transport of >200 keV electrons across the bow shock, the data acquired during the 12-hour periods before and after the shock crossing were subdivided into 3-hour bins, and the counts contributed by the individual samples within each bin were combined by sector. To minimize the effect of the isotropic background (mostly Jovian electrons), which has an intensity level $\lesssim 0.1$ $(\text{cm}^2\ \text{s}\ \text{sr})^{-1}$, only samples with intensity ≥ 0.32 $(\text{cm}^2\ \text{s}\ \text{sr})^{-1}$ were included in this averaging procedure. The resulting average angular distributions and corresponding streaming directions, plotted in Figure 8 at the average position represented by the samples in each 3-hour bin, demonstrate clearly that >200 keV electrons in the outer magnetosheath stream toward the bow shock on average. The magnitude of the anisotropy just inside the shock is $\xi = 0.063 \pm 0.003$. Although this is small, it is 20 standard deviations removed from zero. At the innermost portion of the magnetosheath shown in Figure 8, the streaming is predominantly tailward with a small dawnward component. This is similar to the streaming direction observed in the dawn magnetopause electron layer [*Baker and Stone,* 1978], which results from the draping of magnetic field lines over the magnetosphere. As the bow shock is approached, the streaming vector gradually shifts to the dawnward direction, then becomes sunward along the general Parker spiral direction in the upstream region. This shift of streaming direction through the magnetosheath and across the shock is qualitatively similar to the shift of the magnetic field azimuth in these regions that is predicted by gasdynamic theory [*Alksne,* 1967].

The streaming data presented in Figure 8 support the interpretation that the source of upstream electrons lies in the inner magnetosheath or the magnetosphere. An additional implication of this interpretation is that the net flow of electrons toward the shock in the magnetosheath should equal the observed net flow away from the shock in the upstream region. The net flow F of particles along the field line is $F = 4\pi j\xi/3$. However, because the field changes direction at the shock, it is the component of F along the shock normal which should be continuous across the shock. Thus, if the shock is not a source for these electrons, then the quantity $F \cos \eta$ where η is the angle between the streaming direction and the shock normal, should be the same in the magnetosheath as it is upstream.

Figure 9 presents graphs of average intensity, anisotropy, and net flux normal to the shock for each of the 3-hour bins described above. The plotted intensity represents an average over bursts of intensity ≥ 0.32 $(\text{cm}^2\ \text{s}\ \text{sr})^{-1}$ multiplied by the probability of observing such a burst. For the purpose of calculating the net normal flux $F \cos \eta$, the angle η was taken to be $\varphi_s - \varphi_n$, where φ_s is the azimuth of the observed streaming direction, and where the azimuth of the shock normal φ_n was taken to be 300°, a value appropriate for the ecliptic plane at $X_{GSE} = -13\ R_E$ according to the 'unnormalized' shock of *Formisano* [1979*b*]. According to Figure 9, the average anisotropy in the outer magnetosheath is ~0.06, which is somewhat lower than the results of Figure 7 would suggest. In large part, this is because the measured anisotropies of individual samples are exaggerated by statistical effects, as noted above. These effects are negligible for the angular distributions of Figure 8 and anisotropies of Figure 9, which are based on ≥100,000 counts each. A second reason is that the anisotropy of Figure 9 corresponds to a vector average of the flux contributed by the individual samples. Because the individual samples have a wide distribution in streaming direction, as indicated in Figure 7, this

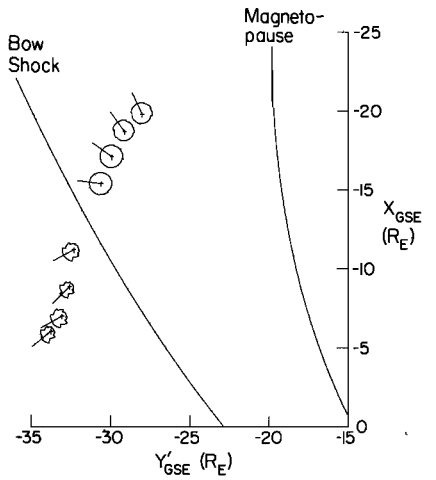

Fig. 8. Average angular distributions of >200 keV electrons in the vicinity of the dawn shock during the period 1973 day 303 to 1977 day 184. The streaming direction corresponding to each angular distribution is indicated by a line originating at the center of the distribution. Spacecraft positions have been rotated into the ecliptic plane (Y_{GSE}' is defined as in Figure 6).

vector average is significantly lower than the average of the magnitudes of the anisotropies. However, since flux is a vector quantity, a vector average is appropriate for determining the average net flux in a given direction.

Figure 9 shows that the average electron intensity and anisotropy both change abruptly at the shock. Relative to the corresponding magnetosheath values, the upstream intensity is reduced by a factor of ~10 and the upstream anisotropy is enhanced by a similar factor. The sudden drop in intensity may be simply explained in terms of the sudden change in magnetic field magnitude at the shock. To show this, it will be assumed that pitch angle scattering in the upstream region is negligible and that the change in field at the shock is gradual enough that $\sin^2 \theta/B$ is conserved, where θ is pitch angle and B is field magnitude. If the magnetosheath particle distribution is approximated by an isotropic phase space density f_0, then, according to Liouville's theorem, the upstream distribution is

$$\begin{aligned} f(\mu) &= f_0 \qquad \mu > (1-\beta)^{1/2} \\ f(\mu) &= 0 \qquad \mu < (1-\beta)^{1/2} \end{aligned} \tag{10}$$

where $\mu = \cos\theta$ and β is the ratio of the upstream field magnitude to the magnetosheath field magnitude. For a typical value $\beta = 0.5$, this implies that particles in the upstream region are restricted to pitch angles <45°. Although the upstream angular distributions shown in Figure 8 do exhibit a high degree of collimation, particles are observed at all pitch angles. Evidently the assumptions of scatter-free transport in the upstream region and conservation of $\sin^2 \theta/B$ at the shock are useful approximations, but are not valid exactly. The ratio of upstream intensity j_u to magnetosheath intensity j_s implied by this calculation is

$$\frac{j_u}{j_s} = \frac{\int_{(1-\beta)^{1/2}}^{+1} f_0 \, d\mu}{\int_{-1}^{+1} f_0 \, d\mu} = \frac{1-(1-\beta)^{1/2}}{2} \tag{11}$$

For $\beta = 0.5$, this ratio is 0.15 which is fairly close to the observed value 0.1. The small remaining discrepancy might be caused by tilting of the magnetic field out of the ecliptic plane. Such tilting would cause the detector, which scans the ecliptic plane, to miss a portion of the collimated upstream distribution, thus reducing the observed upstream intensity. The observed magnetosheath intensity, on the other hand, would be little affected by field tilting, since the magnetosheath distribution is nearly isotropic. The calculation given above is similar to one given by *Palmer* [1981], except that Palmer considered the case where transport is scatter-free in the magnetosheath as well as in the upstream region, an assumption not justified by the nearly isotropic magnetosheath angular distributions shown in Figure 8.

The major point to note in Figure 9 is that although the intensity and anisotropy both change sharply at the shock, these two changes counterbalance in such a way that the net flux normal to the shock $F \cos\eta$ is very nearly the same in the magnetosheath and upstream. For the 3-hour bin just inside the magnetosheath, the net normal flux is 0.17 $(cm^2\ s)^{-1}$, and for the 3-hour bin just outside the shock it is 0.15 $(cm^2\ s)^{-1}$. This net flux remains fairly constant as the spacecraft progresses farther into the upstream region. There is no evidence of an enhanced flux contributed by the shock. Although the magnetosheath bins from −9 to −6 hours and from −6 to −3 hours also have normal fluxes which are similar to the fluxes observed in the bins immediately adjacent to the shock, this agreement may be fortuitous. These more inward bins probably correspond to field lines that cross the shock some distance tailward, and the locally observed streaming direction may not reflect the streaming direction at the point these particles cross the shock. In fact, for the innermost bin the formally computed net normal flux is negative and for that reason is not plotted.

The close agreement of net fluxes on either side of the

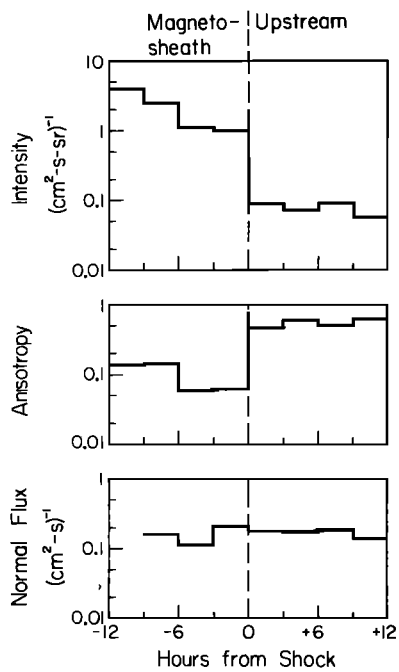

Fig. 9. Intensity, anisotropy, and component of net flux normal to the shock of >200 keV electrons as a function of time from shock crossing. Bins correspond to the angular distributions depicted in Figure 8.

shock is much stronger evidence for a magnetosheath source than is the simple fact that the intensity is higher in the magnetosheath. Although a higher intensity observed in some region suggests that the region may be nearer the source, it is only through a calculation of the net flux that the source location can be definitely established. For example, if, in the calculation above, the intensity in the magnetosheath had been only twice the upstream intensity, then, as a result of the much larger anisotropies seen upstream, the upstream flux would have been substantially larger than the magnetosheath flux. It would then have been necessary to conclude that the shock is a major source of these particles, even though a greater intensity is observed in the magnetosheath. The observation that the net fluxes in the magnetosheath and upstream are, in fact, equal demonstrates conclusively that it is the magnetosheath population of energetic electrons that supplies the upstream bursts.

MEAN FREE PATH OF >200 KEV ELECTRONS IN THE OUTER MAGNETOSHEATH

The nearly isotropic angular distributions observed in the outer magnetosheath differ markedly from the collimated ones observed upstream, as illustrated in Figure 8. This suggests that pitch angle scattering of >200 keV electrons is far more intense in the magnetosheath than upstream. The leaky box model of energetic particle transport, which describes particle transport in a region of intense scattering bounded by a region of little or no scattering, may thus apply to energetic electrons in Earth's magnetosheath. In this model the flux F supplied by sources within a box (the magnetosheath) of length scale L is balanced by the free escape of particles across a boundary (the bow shock) on a time scale τ. The equation that describes this equilibrium is

$$\frac{\partial n}{\partial t} = \frac{F}{L} - \frac{n}{\tau} = 0 \qquad (12)$$

where n is density and t is time. Noting that $F = nW\xi/3$, where W is the particle velocity, this implies that $\tau = 3L/W\xi$. The velocity of a 200 keV electron is $\sim 0.7c$, and, from Figure 9, the anisotropy in the outer magnetosheath is $\xi \sim 0.06$. Taking $L \sim 10\ R_E$ for the length scale of the magnetosheath, the escape time of >200 keV electrons is $\tau \sim 15$ s. The parallel diffusion coefficient implied by this escape time and length scale is $K_{\parallel} = L^2/\tau \sim 2.7 \times 10^{18}$ cm^2 s^{-1}, which corresponds to a mean free path $\lambda = 3K_{\perp}/W \sim 0.6\ R_E$. This value agrees well with the average mean free path of 1 R_E obtained independently by *Palmer* [1981], who utilized the same data set but a different analytical approach, and who concluded that this value is consistent with the mean free path predicted by quasilinear scattering theory from observed magnetosheath magnetic fluctuation spectra. Additional implications of the leaky box model are that an electron is scattered ~300 times in the course of traversing the magnetosheath, and that a diffusive gradient $\sim 10\%/R_E$ is required to drive the observed flow.

DISCUSSION

The >200 keV electrons studied in this report are unrelated to the 1.5 to >16 keV electrons studied by *Anderson et al.* [1979]. These lower energy electrons are observed in thin sheets just downstream of interplanetary field lines that are tangent to the bow shock, and are believed to be solar wind electrons accelerated by an interaction with the bow shock. The dependence of these shock-associated electrons upon field geometry differs radically from the dependence of the >200 keV electrons, which flow across the shock near the dawn meridian and emerge onto interplanetary field lines that normally intersect the shock at an angle around 90°. Considerable evidence has been presented here to show that the >200 keV electrons are not shock-associated, but rather that they originate downstream of the shock and are probably related to the magnetopause electron layer.

The existence of two distinct sources complicates the interpretation of upstream energetic electron data. The results presented here show that >200 keV shock-accelerated electrons, if they exist at all, are very small in number compared to >200 keV electrons that originate downstream, although *Anderson et al.* [1979] suggest that shock-accelerated electrons do extend to ~100 keV. At lower energies, the relative contribution of the two sources is difficult to assess on the basis of published information. A downward extrapolation of the >200 keV intensity suggests that typical intensities of electrons originating downstream of the shock should be well above the threshold of the detectors utilized by Anderson et al. However, these detectors are oriented perpendicular to the ecliptic plane, and hence might selectively exclude collimated, field-aligned fluxes of the type reported here even if such fluxes do extend downward in energy to ~10 keV. In earlier work, *Anderson* [1968, 1969] studied >40 keV upstream electrons and concluded that they were shock-associated. A downward extrapolation of the energy spectrum of upstream >200 keV electrons suggests that the integral intensity at 40 keV would be in the range of 10 to 3000 (cm^2 s sr)$^{-1}$. This is very similar to the range of upstream burst intensities observed by Anderson at 40 keV. Furthermore, *Anderson* [1969] computed an integral power law exponent of 1.8 for 22 to 45 keV electrons, corresponding to a differential power law exponent of 2.8. This is close to the value 3.2 obtained for the higher energy electrons studied here. It thus seems possible that some of the upstream bursts observed by Anderson were the low energy extension of the electrons studied here, which originate downstream of the shock. A definitive conclusion concerning the relative contribution of the two sources of upstream electrons as a function of energy must await further study.

SUMMARY AND CONCLUSIONS

This report has described in detail the properties of >200 keV electron bursts upstream of the bow shock and in the outer magnetosheath. In the upstream region, the bursts have intensities ranging from near the background level ~0.1 (cm^2 s sr)$^{-1}$ up to ~100 (cm^2 s sr)$^{-1}$. Intensity levels ≥0.32 (cm^2 s sr)$^{-1}$ are observed about 2% of the time. Individual bursts typically last less than 5 min. The electrons stream intensely ($\xi \sim 0.5$ to 1.5) in the sunward direction along the interplanetary field line and are characterized by an energy spectral index $\gamma \sim 3.2$. Bursts in the outer magnetosheath have time scales and spectral indices similar to those observed upstream, but they are typically ~10 times more intense and much less anisotropic ($\xi \lesssim 0.4$). Their streaming direction shifts from predominantly tailward to predominantly dawnward as the bow shock is approached, consistent

with the flow direction observed upstream when the distortion of the field in the magnetosheath is taken into account. The mean free path of >200 keV electrons in the outer magnetosheath, determined by treating the magnetosheath as a leaky box with the bow shock serving as a free escape boundary, is $\sim 0.6\ R_E$.

A principal conclusion of this report is that the upstream energetic electrons are closely related to those in the permanent layer of energetic electrons adjacent to the magnetopause. Upstream bursts are far more sporadic and infrequent than bursts in the layer, but this is principally due to the fact that for most interplanetary field configurations, a spacecraft in the upstream region is not favorably connected to the inner magnetosheath along the field line, an effect than can be quantified with the aid of the GIPM coordinate system. Upstream bursts are most frequently observed at $Y_{GIPM} < 0$ on field lines with small values of $|Z_{GIPM}|$. These field lines probe deeply into the magnetosheath and are most probably the sunward extension of the field lines threading the magnetopause electron layer.

Quantitative support for these conclusions was obtained with the aid of average values of net flux obtained from nearly 4 years of data. In the outer magnetosheath the component of net flux normal to the bow shock is directed toward the shock and is nearly equal in magnitude to the net normal flux away from the shock in the adjacent upstream region. In addition, the total number of >200 keV electrons streaming away from Earth in the upstream region accessible to IMP 8 is $\sim 2.7 \times 10^{20}$/s, which corresponds to a total average energy flow $\sim 1.6 \times 10^{14}$ ergs/s. This figure is typical of the total energy transported tailward by >200 keV electrons in the magnetopause electron layer [*Baker and Stone, 1977b*].

Acknowledgments. We thank R. P. Lepping and N. F. Ness for generously providing IMP 8 magnetometer data through the National Space Science Data Center. We are grateful to R. E. Vogt, who has been closely associated with this investigation, and to W. E. Althouse, D. N. Baker, G. J. Hurford, J. E. Lupton, and R. A. Mewaldt, who made significant contributions to various phases of this program. This work was supported in part by the National Aeronautics and Space Administration under contracts NAS5-11066 and NAS5-25789 and grant NGR 05-002-160.

The Editor thanks V. Domingo and R. P. Lin for their assistance in evaluating this paper.

REFERENCES

Alksne, A. Y., The steady-state magnetic field in the transition between the magnetosphere and the bow shock, *Planet. Space Sci., 15,* 239, 1967.

Anderson, K. A., Energetic electrons of terrestrial origin upstream in the solar wind, *J. Geophys. Res., 73,* 2387, 1968.

Anderson, K. A., Energetic electrons of terrestrial origin behind the bow shock and upstream in the solar wind, *J. Geophys. Res., 74,* 95, 1969.

Anderson, K. A., R. P. Lin, F. Martel, C. S. Lin, G. K. Parks, and H. Rème, Thin sheets of energetic electrons upstream from the earth's bow shock, *Geophys. Res. Lett., 6,* 401, 1979.

Baker, D. N., and E. C. Stone, The magnetopause electron layer along the distant magnetotail, *Geophys. Res. Lett., 4,* 133, 1977*a*.

Baker, D. N., and E. C. Stone, The relationship of energy flow at the magnetopause to geomagnetic activity, *Geophys. Res. Lett., 4,* 395, 1977*b*.

Baker, D. N., and E. C. Stone, Observations of energetic electrons ($E \gtrsim 200$ keV) in the earth's magnetotail: Plasma sheet and fireball observations, *J. Geophys. Res., 82,* 1532, 1977*c*.

Baker, D. N., and E. C. Stone, The magnetopause energetic electron layer, 1, Observations along the distant magnetotail, *J. Geophys Res., 83,* 4327, 1978.

Bieber, J. W., and E. C. Stone, Energetic electron bursts in the magnetopause electron layer and in interplanetary space, in *Proceedings of Magnetospheric Boundary Layers Conference, ESA Spec. Publ. 148* edited by B. Battrick and J. Mort, p. 131, European Space Agency, Neuilly, France, 1979.

Domingo, V., D. E. Page, and K.-P. Wenzel, Energetic and relativistic electrons near the polar magnetopause, *J. Geophys. Res., 82,* 2327, 1977.

Fan, C. Y., G. Gloeckler, and J. A. Simpson, Evidence for >30-keV electrons accelerated in the shock transition region beyond the earth's magnetospheric boundary, *Phys. Rev. Lett., 13,* 149, 1964.

Formisano, V., Properties of energetic electrons of magnetospheric origin in the magnetosheath and in the solar wind—Correlation with geomagnetic activity, *Planet. Space Sci., 27,* 867, 1979*a*.

Formisano, V., Orientation and shape of the earth's bow shock in three dimensions, *Planet. Space Sci., 27,* 1151, 1979*b*.

Formisano, V., V. Domingo, and K.-P. Wenzel, The three-dimensional shape of the magnetopause, *Planet. Space Sci., 27,* 1137, 1979.

Gosling, J. T., J. R. Asbridge, S. J. Bame, G. Paschmann, and N. Sckopke, Observations of two distinct populations of bow shock ions in the upstream solar wind, *Geophys. Res. Lett., 5,* 957, 1978.

Krimigis, S. M., D. Venkatesan, J. C. Barichello, and E. T. Sarris, Simultaneous measurements of energetic protons and electrons in the distant magnetosheath, magnetotail, and upstream in the solar wind, *Geophys. Res. Lett., 5,* 961, 1978.

Lin, R. P., C.-I. Meng, and K. A. Anderson, 30- to 100-keV protons upstream from the earth's bow shock, *J. Geophys. Res., 79,* 489, 1974.

Marshall, F. E., The streaming of 1.3–2.3 MeV cosmic-ray protons during periods between prompt solar particle events, Ph.D. thesis, Calif. Inst. of Technol., Pasadena, 1977.

Meng, C.-I., and K. A. Anderson, A layer of energetic electrons (>40 keV) near the magnetopause, *J. Geophys. Res., 75,* 1827, 1970.

Meng, C.-I., and K. A. Anderson, Characteristics of the magnetopause energetic electron layer, *J. Geophys. Res., 80,* 4237, 1975.

Palmer, I. D., Propagation of energetic electrons in the magnetosheath and upstream solar wind, *J. Geophys. Res., 86,* 4461, 1981.

Paschmann, G., N. Sckopke, J. R. Asbridge, S. J. Bame, and J. T. Gosling, Energization of solar wind ions by reflection from the earth's bow shock, *J. Geophys. Res., 85,* 4689, 1980.

Sarris, E. T., S. M. Krimigis, and T. P. Armstrong, Observations of magnetospheric bursts of high-energy protons and electrons at $\sim 35\ R_E$ with IMP 7, *J. Geophys. Res., 81,* 2341, 1976.

Scholer, M., G. Gloeckler, F. M. Ipavich, D. Hovestadt, and B. Klecker, Pitch angle distributions of energetic protons near the earth's bow shock, *Geophys. Res. Lett., 6,* 707, 1979.

Sonnerup, B. U. O., Acceleration of particles reflected at a shock front, *J. Geophys. Res., 74,* 1301, 1969.

Stone, E. C., D. N. Baker, and E. W. Hones, Fast electrons near the magnetopause and their dependence on interplanetary parameters (abstract), *Eos Trans. AGU, 59,* 365, 1978.

Zwickl, R. D., S. M. Krimigis, T. P. Armstrong, and L. J. Lanzerotti, Ions of Jovian origin observed by Voyager 1 and 2 in interplanetary space, *Geophys. Res. Lett., 7,* 453, 1980.

(Received May 4, 1981;
revised July 1, 1981;
accepted July 1, 1981.)